frontiers in Marine Science

ORIGINAL RESEARCH
published: 06 October 2020
doi: 10.3389/fmars.2020.586281

Distribution of Select Cement Proteins in the Acorn Barnacle *Amphibalanus amphitrite*

Janna N. Schultzhaus[1†‡], Chenyue Wang[2†], Shrey Patel[3], Madeline Smerchansky[3], Daniel Phillips[4‡], Chris R. Taitt[5], Dagmar H. Leary[5], Judson Hervey[5], Gary H. Dickinson[6], Christopher R. So[7], Jenifer M. Scancella[7‡], Kathryn J. Wahl[7] and Christopher M. Spillmann[5]*

[1] National Research Council Research Associateship Program, National Academy of Science, Engineering, and Medicine, Washington, DC, United States, [2] George Mason University, Fairfax, VA, United States, [3] Naval Research Enterprise Internship Program, American Society for Engineering Education, Washington, DC, United States, [4] American Society for Engineering Education, Washington, DC, United States, [5] Center for Bio/Molecular Science and Engineering, U.S. Naval Research Laboratory, Washington, DC, United States, [6] Department of Biology, The College of New Jersey, Ewing, NJ, United States, [7] Chemistry Division, U.S. Naval Research Laboratory, Washington, DC, United States

OPEN ACCESS

Edited by:
Andrew Stanley Mount,
Clemson University, United States

Reviewed by:
Tara Essock-Burns,
University of Hawaii, United States
Nick Aldred,
Newcastle University, United Kingdom
Guoyong Yan,
Institute of Deep-Sea Science and Engineering (CAS), China

***Correspondence:**
Christopher M. Spillmann
christopher.spillmann@nrl.navy.mil

[†] These authors have contributed equally to this work

[‡]Present address:
Janna N. Schultzhaus, Center for Bio/Molecular Science and Engineering, U.S. Naval Research Laboratory, Washington, DC, United States
Daniel Phillips, U.S. Army Combat Capabilities Development Command (CCDC), Chemical Biological Center, Oak Ridge Institute for Science and Education, Aberdeen, MD, United States
Jenifer M. Scancella, Navy Drug Screening Laboratory (NDSL), Jacksonville, FL, United States

Specialty section:
This article was submitted to Marine Molecular Biology and Ecology, a section of the journal Frontiers in Marine Science

Received: 23 July 2020
Accepted: 31 August 2020
Published: 06 October 2020

Acorn barnacles are major marine fouling organisms. Their success is largely due to an ability to adhere to diverse substrates via a sub-micron thick proteinaceous adhesive layer that develops as the organism molts and expands its base. Recent work has expanded the set of proteins identified within the adhesive interface, but one outstanding question concerns their spatial distribution throughout the organism. Here, we employ immunological analysis of *Amphibalanus amphitrite* tissue sections and identify the presence of two cement proteins, AaCP19-1 and AaCP43-1, in areas far removed from the adhesive interface. Confocal imaging reveals specific staining along different tissue linings of the organism as well as other non-cementing regions. Additionally, we employ a modified, pressure cycling technology approach to recover protein from histological tissue sections to perform proteomics analysis. Mass spectrometry analysis of proteins recovered from transverse histological sections of the upper portion of barnacles indicates the presence of these same proteins, complementing the immunostaining observations. The proteomics analysis also revealed the presence of other proteins first identified in the adhesive layer. While some proteins are clearly enriched at the surface interface, our findings challenge the concept that cement proteins are exclusive to the substrate interface and suggest they may have an expanded physiological role beyond substrate adhesion-related processes of *A. amphitrite*.

Keywords: acorn barnacle, barnacle cement, cement protein, tissue sections, confocal microscopy, mass spectrometry

INTRODUCTION

As a major marine macrofouler, acorn barnacles adhere to a variety of surfaces via a proteinaceous adhesive, commonly referred to as barnacle cement. This cement is a secreted material (Dickinson et al., 2009) that transitions to a recalcitrant and permanent solid in the mature form (Naldrett, 1993; Naldrett and Kaplan, 1997; Kamino et al., 2000). During the last three decades, a number

of unique proteins in the adhesive have been identified (Kamino et al., 1996, 2000; Naldrett and Kaplan, 1997; Jonker et al., 2014; Lin et al., 2014; Wang et al., 2015; So et al., 2016, 2017; Rocha et al., 2018; Schultzhaus et al., 2019). Historically, the majority of research groups have designated these proteins as "cement proteins" based on their location of isolation. No experimental validation of the adhesive properties of specific barnacle proteins has been demonstrated to date, although several biochemical mechanisms for adhesion have been proposed, including: hydrophobic forces produced by high levels of aliphatic residues (Naldrett, 1993; Naldrett and Kaplan, 1997; Kamino et al., 2012; Kamino, 2013; Jonker et al., 2014); repetitive sequence motifs similar to those found in silk proteins (So et al., 2016) promoting nanofibril formation (Barlow et al., 2010; Burden et al., 2014; Nakano and Kamino, 2015; Fears et al., 2018; So et al., 2019); protein polymerization as a specialized form of wound healing (Dickinson et al., 2009); and post-translational modifications via oxidation (So et al., 2017). In addition to a lack of experimental verification of their adhesive properties, the function of cement proteins beyond a potential role in adhesion at the interface has not been examined. Understanding the distribution of these proteins could shed light on whether they have an expanded biological role in cirripedes.

Our understanding of where cement proteins are synthesized in acorn barnacles and how they make their way to the interface remains incomplete. In stalked barnacles, the stretched anatomy combined with the lack of an obscuring calcareous shell over the stalk has allowed observation via histology, thereby promoting a more informed insight into the production mechanism of proteins found in the adhesive (Power, 2010). In acorn barnacles, conversely, the region where cement is deposited at the leading edge of the basis is confined to a thickness on the order of microns and obscured beneath calcareous parietal plates. Historically, release of acorn barnacle cement has been attributed to cement glands located in the sub-mantle tissue and distributed to the interface via a radial capillary network (Darwin, 1854; Lacombe and Liguori, 1969; Lacombe, 1970; Saroyan et al., 1970; Walker, 1970). The cement glands have been described as being distributed amongst the ovaries; they have been identified due to their distinct morphological and staining profile (Lacombe and Liguori, 1969; Lacombe, 1970; Fyhn and Costlow, 1976; He et al., 2018). Little direct biochemical evidence exists to link the acorn barnacle cement glands to the actual *deposition* of cement at the leading interfacial growth edge, aside from a recent report indicating the presence of a particular cement protein, Aa-cp100k, in *Amphibalanus amphitrite* cement glands (He et al., 2018).

Some important insights into the surface preparation and growth process at the basis leading edge have been gained through confocal microscopy observations of live specimens on glass coverslips (Burden et al., 2014; Fears et al., 2018). Fears et al. (2018) used confocal microscopy with fluorescent labels against several biomacromolecules to better understand the composition of the barnacle-substrate interface as it developed over the course of a molt cycle. Nanofibrils associated with the adhesive layer were observed in the leading edge region where the capillary network had not yet formed, providing indirect evidence that initial formation of the adhesive interface may occur independently of the capillary network and, therefore, the cement glands. In addition, a layer of cells was observed within 20 microns of the leading edge, indicating these cells may contribute to the deposition of adhesive proteins at the interface (Fears et al., 2018). These results stress how much remains to be understood about the mechanism of cement production in adult acorn barnacles.

In terms of the *composition* of the protein adhesive, only a handful of proteins were initially isolated and identified from acorn barnacles (Kamino et al., 1996, 2000; Naldrett and Kaplan, 1997), especially in the representative fouling species *Amphibalanus* (=*Balanus*) *amphitrite* (Clare and Rittschof, 1989; Pitombo, 2004; Clare and Høeg, 2008). A few reports have also claimed the uniqueness of select proteins to the basal region in the acorn barnacle *Megabalanus rosa* using gross dissection (Kamino et al., 2000; Urushida et al., 2007). More recently, our group has identified over 80 proteins in the adhesive of *A. amphitrite* using both transcriptomics (Wang et al., 2015) and proteomics approaches (So et al., 2016, 2017; Schultzhaus et al., 2019). With an abundance of proteins identified from the cement, we now seek answers to fundamental questions regarding these materials: are proteins first identified in the adhesive interface in *A. amphitrite* unique to the adhesive layer? If not, what is their distribution within the barnacle? Using a combination of immunofluorescence confocal microscopy, western blotting, and proteome profiling of formalin fixed paraffin embedded (FFPE) sections, we primarily focus on the distribution of two prominent proteins found in barnacle cement, AaCP19-1 and AaCP43-1, and then expand our findings to other proteins associated with the cement layer of *A. amphitrite*. The combined body of evidence (in this study and published previously) indicate many proteins first identified in barnacle cement are enriched in the adhesive as previously observed. However, our recent observations call into question the exclusivity of cement proteins to the cement of *A. amphitrite* and suggest they may have an expanded physiological role beyond adhesion to an underlying substrate.

MATERIALS AND METHODS

Primary Antibodies

Polyclonal antibodies against cement proteins AaCP19-1 and AaCP43-1 were generated in rabbit by GenScript, Inc. (Piscataway, NJ, United States). Antibodies directed against *A. amphitrite* proteins were labeled with Cy5 mono-*N*-hydroxysuccinimidyl (GE Healthcare Amersham CyDye mono-reactive dye 5-packs, # PA25001; VWR, Radnor, PA, United States) essentially as previously described (Taitt et al., 2009). Antibody [0.5 mg, in phosphate-buffered saline (PBS)] was diluted to 0.5 mg/mL in 50 mM sodium bicarbonate pH 8.5. Five microliters of Cy5 dye (one packet, previously dissolved in 30 uL anhydrous DMSO) was then added and the reaction incubated for 45 min at room temperature, with intermittent mixing. Unincorporated dye was removed via Zeba desalting spin columns (40K MWCO, Thermo Fisher

Scientific, Waltham, MA, United States). Cy5- and horseradish peroxidase- (HRP-) conjugated secondary antibodies were obtained from Jackson ImmunoResearch, Inc. (West Grove, PA, United States).

Gel Electrophoresis and Immunoblotting

Opaque cement collections, sodium dodecyl sulfate-polyacrylamide gel electrophoresis (SDS-PAGE), and immunoblotting were performed as described previously (So et al., 2017). Briefly, opaque glue (Wendt et al., 2006), also referred to as gummy cement (Ramsay et al., 2008; Dickinson et al., 2009), was collected from adult *A. amphitrite* and solubilized in hexafluoroisopropanol (HFIP). Solubilized cement proteins were transferred to a 1.5 mL polypropylene tube and evaporated to dryness by vacuum centrifuge (Labconco, Kansas City, MO, United States). Dried samples were immediately suspended in Laemmli sample buffer containing 300 mM dithiothreitol (DTT) and heated for 15 min at 95°C. Samples were then loaded onto precast gels (Any kD Mini-PROTEAN TGX, Bio-Rad, Hercules, CA, United States) and separated by SDS-PAGE under constant voltage. Gels were stained with Imperial protein stain (Thermo Fisher Scientific) according to manufacturer instructions and imaged using a gel box (UVP ChemiDoc-it, Upland, CA, United States).

For immunoblotting, unstained PAGE gels were transferred to PVDF membranes (Sequi-Blot, 0.22 μm, Bio-Rad) using a western transfer wet cell (Mini Trans-Blot cell, Bio-Rad, Hercules, CA, United States) at constant voltage (100 V) for 2 h in Tris-glycine-methanol transfer buffer with an ice block. The membrane was blocked with 2.5% instant milk and probed with 10 μg/mL rabbit anti-AaCP-19-1 (Genscript USA, Piscataway, NJ, United States) in PBS pH 7.3 containing 0.05% Tween-20 and 1 mg/mL BSA (PBSTB). AaCP19-1 antigen (Genscript USA, Piscataway, NJ, United States) was loaded as a positive control. Primary antibodies were detected with HRP-goat anti-rabbit IgG antibody (H + L) (Invitrogen) and visualized using enhanced chemiluminescence (ECL) western blotting substrate (Thermo Fisher Scientific, Waltham, MA, United States) and ChemiDoc Imager (Bio-Rad, Hercules, CA, United States). The corresponding secondary antibody was used at 1:10,000 dilution, using the same blocking method as above.

Histological Section Preparation

The FFPE sections of *A. amphitrite* were prepared by Mass Histology Inc. and the Histopathology and Tissue Shared Resource at Georgetown University Medical Center (Washington, DC, United States). Briefly, whole *A. amphitrite* grown on glass or reattached (Rittschof et al., 2008) on paraffin film or Histogel (Thermo Fisher Scientific, Waltham, MA, United States) substrates were sterilized in 70% ethanol with the substrate intact, then demineralized for 2–3 days using Immunocal (StatLab, KcKinney, TX, United States; 12% formic acid) and fixed with 10% formalin for 24 h. The fixed and decalcified tissue was embedded in paraffin and sliced in either a transverse or sagittal orientation to create a series of 5–7 μm-thick sections.

Immunohistochemistry

Formalin fixed paraffin embedded sections were briefly immersed in xylene. The resulting deparaffinized sections were rehydrated with a decreasing gradient of ethanol from 100 to 50%. For antigen retrieval, the rehydrated tissue sections were boiled in 0.1 M sodium citrate buffer, pH 6.0 for 40 min. After being rinsed with Tris-buffered saline (TBS) pH 7.6, the sections were blocked using 10 mg/mL BSA and then incubated with the Cy5-conjugated primary or secondary antibodies either at 4°C overnight or at room temperature for 90 min. The sections were rinsed again and incubated with 200 ng/mL 4′,6-diamidino-2-phenylindole (DAPI) in TBS at room temperature for 30 min and mounted with Aqua poly/Mount (Polysciences Inc., Warrington, PA, United States).

Confocal Microscopy Imaging

Microscopy was performed on a Nikon A1RSi Laser Scanning Confocal Imaging system and a Zeiss LSM800 system. Standard settings for DAPI (Ex: 405 nm, Em: 450/50 nm), fluorescein (Ex: 488 nm, Em: 525/50 nm), and Cy5 (Ex: 647 nm, Em: 685/50 nm) were used to image. The fluorescein channel was used to monitor previously documented autofluorescence (Burden et al., 2012, 2014). Sequential imaging of each channel, i.e., a channel series, was performed to minimize fluorescence bleed-through across the emission channels. Image settings, including laser power and gain, were set according to control sections incubated with only Cy5-labeled secondary antibodies. This excluded the base region of the barnacle (in both transverse and sagittal sections), which showed non-specific binding and similar signal intensity for all antibodies labeled with Cy5. The imaging software used was either Nikon Elements or Zeiss Zen.

Proteomic Analysis of FFPE Histological Tissue Sections

Three types of sections were initially processed as described in section "Histological Section Preparation", then used for proteomics analysis: Sagittal + Basal Transverse (S + BT); Lower Transverse (LT); and Upper Transverse (UT) (**Figures 1**, **5A**). The S + BT group was created by first bisecting an individual barnacle from the operculum to the base plate and then orienting the halves so that one was used to produce sagittal sections while the other was used to produce transverse sections. Two adjacent pairs of these sections were analyzed: the sagittal section from the middle of the barnacle, containing the main body and sub-mantle tissue, and the transverse section within several microns of the barnacle base, containing the cuticular material near the substrate interface and accompanying cement material. Two pairs of the S + BT groupings were processed (four sections total). The LT groupings were collected from tissue immediately above the base plate (∼ tens of microns from the barnacle base). Each contained three pooled adjacent transverse sections from the barnacles, with a total of four samples processed (12 sections total). The UT group was collected from tissue near the upper parietal shells but below the operculum (open top of the barnacle shell and typically hundreds

of microns from the barnacle base). Each also contained three pooled transverse sections from three individual barnacles (nine sections total).

Formalin fixed paraffin embedded tissue sections were prepared for proteome profile analysis by liquid chromatography tandem mass spectrometry (LC-MS/MS) with analytical-grade reagents (Fisher Optima grade, etc.). A method for protein sample recovery from FFPE sections (Föll et al., 2018) was adapted for use with pressure cycling technology (PCT) (Tao et al., 2007; López-Ferrer et al., 2008) for barnacle protein extracts as previously described (Fears et al., 2018; Wang et al., 2018; Schultzhaus et al., 2019). Tissue area was measured and sections were deparaffinized and rehydrated (3 × 5 min in xylene; 2 × 5 min in 99% EtOH; 20 s each in 99, 96, 70, and 50% EtOH) and scraped off glass slides into 1.5-mL protein low-bind Eppendorf tubes. 200 μL of heat induced antigen retrieval buffer [HIARB: 0.1% Rapigest SF (Waters, Milford, MA, United States), 1 mM DTT, 0.1 M ammonium bicarbonate (substituted for HEPES)] per 100 mm^2 of tissue was added. Heat induced antigen retrieval was performed at 95°C and centrifuged at 750 rpm for 4 h. PCT-enhanced enzymatic proteolysis was performed in a Barocycler NEP 2320 with addition of 2 μg sequencing-grade modified trypsin (Promega V5111, Madison, WI, United States) per mm^3 of tissue. The Barocycler NEP 2320 performed sample digestion into peptides at 45,000 psi, 50°C (for v_f = 150 μL). Pressure was applied at 50-s intervals with 10-s depressurization pauses for 1.5 h per sample. Cellular debris was sedimented from peptide samples (19,000 g, 15 min) and the supernatant removed for further processing. Disulfide bonds were treated with the addition of 10 mM DTT 15 min at 37°C, 30 mM iodoacetamide for 15 min at 37°C, 10 mM DTT for 15 min at 37°C in the dark. Guanidine chloride was added to a final concentration of 3 M and samples were acidified to pH <3 with pure formic acid. After 30 min incubation at 37°C, samples were spun at 19,000 g for 10 min to remove HIARB. Peptides were desalted with 100-μL C_{18} OMIX tips (Agilent Technologies, Santa Clara, CA, United States), organic elution solvent was removed by Speed-Vac (Savant/Thermo Fisher Scientific, Waltham, MA, United States) and peptides were stored frozen prior to reconstitution in 0.1% formic acid in water (Fisher Optima grade).

For detailed LC and MS instrument settings and data processing protocols, see **Supplementary File S1**. Shotgun proteome profiling by LC-MS/MS was performed with a U3000 HPLC system coupled to an Orbitrap Fusion Lumos Tribrid mass spectrometer (Thermo Fisher Scientific, Waltham, MA, United States) as previously detailed (Dean et al., 2020). The Orbitrap acquired profile (or untargeted) measurements and targeted measurements (**Supplementary Table S1**) for observed mass-to-charge (m/z) ratios in data dependent mode with dynamic exclusion enabled. Mascot (Matrix Science, LTD, London, United Kingdom) and Scaffold (Proteome Software, Portland, OR, United States) were used for peptide-spectrum matching (PSM) of MS/MS spectra to *in silico* predicted proteins.

A limited, manually curated list of 106 predicted barnacle protein sequences based on transcriptomic data from sub-mantle tissue (Wang et al., 2015) was used as the primary sequence database reference, as previously described (So et al., 2016, 2017; Wang et al., 2018). Only proteins previously identified in *A. amphitrite* adhesive (Schultzhaus et al., 2019) and several other likely highly abundant proteins (i.e., actin, collagen, vitellogenin) were included in this reference database as barnacle proteins. These sequences were concatenated with an in-house list of 191 contaminant, mass standard, and reagent peptide sequences (e.g., trypsin, keratins, etc.) (Hervey et al., 2009) for a total of 296 sequences. The heat map of the proteomic data was created using the R package gplots (heatmap.2) (Warnes et al., 2015).

RESULTS

Histological Observations

Histological FFPE sections were prepared to observe the interior anatomy of *A. amphitrite* and to assess the spatial distribution of two cement proteins, AaCP19-1 and AaCP43-1, using fluorescent-labeled, custom polyclonal antibodies with confocal microscopy. Representative hematoxylin and eosin (H&E)-stained transverse and sagittal sections and accompanying diagrams of the major anatomical features are shown in **Figure 1**. In *A. amphitrite*, external calcified plates (parietal on the sides, opercular on the top, and, as with many species, a base plate at the interface) protect all soft tissue. The main body containing the digestive and male reproductive systems is suspended near the opercular opening. *A. amphitrite* are hermaphrodites, and the female reproductive tissue, composed of ovarioles with maturing oocytes, is located in the sub-mantle tissue that lines the base of the barnacle. Some soft tissue is encased within the parietal and base plates (longitudinal and lateral canal tissue). In general, sagittal and transverse sections through the central portion of *A. amphitrite* show four main regions: (i) the main body; (ii) the area below the main body and mantle lining (i.e., the sub-mantle region) that is primarily composed of the ovarioles; (iii) the lateral and longitudinal canals of the parietal and base plates; and (iv) soft tissue in proximity to the substrate interface. Tissues within these four main regions were examined for immunohistological evidence of cement proteins AaCP19-1 and AaCP43-1.

Immunoblotting and Immunofluorescence Confocal Microscopy

As a first step toward understanding the distribution of cement proteins, it was critical to confirm that the polyclonal antibodies bind to specific proteins from *A. amphitrite* adhesive. Previous analysis with immunoblotting has demonstrated both antibodies directed against AaCP19-1 and AaCP43-1 bound to select components of the adhesive of *A. amphitrite* when barnacles were grown on nitrocellulose membranes (So et al., 2019). Further, anti-AaCP43-1 has been shown to interact with specific bands after SDS-PAGE gel separation of solubilized adhesive (So et al., 2017). Here, immunoblotting with anti-AaCP19-1 showed binding to the 19 kDa AaCP19-1 antigen and to a band at ∼20 kDa in solubilized gummy glue (**Supplementary Figure S1**). Bands observed at higher molecular

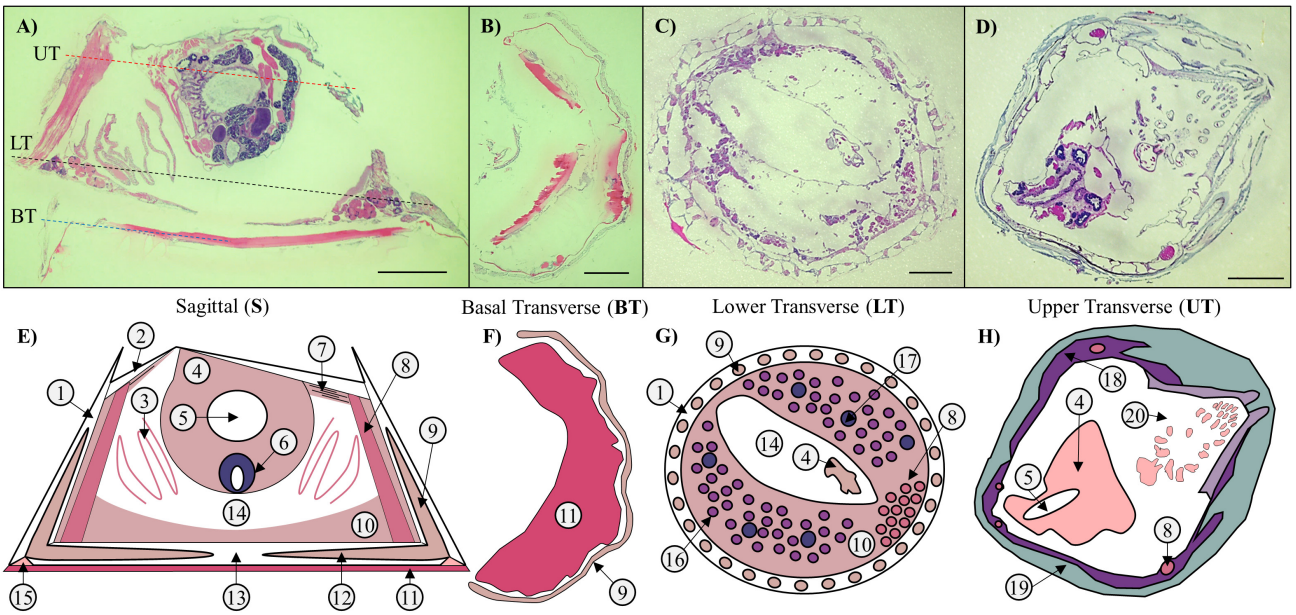

FIGURE 1 | Sections and schematics of *Amphibalanus amphitrite* anatomy. **(A–D)** H&E stained sagittal (S) and transverse sections of a decalcified adult. The dashed lines in panel **(A)** indicate the location of the transverse sections along the sagittal plane: blue = basal transverse (BT) sections of a sagittally bisected individual; black = lower transverse (LT) sections; and red = upper transverse (UT) sections. Sections through the middle of the barnacle of the barnacle contain a collection of most, if not all, types of tissue present in an adult barnacle. **(B)** BT sections are cut through the basal region directly attached to the substrate and below the previous location of base plate, and contain mostly cuticle. **(C)** LT sections are cut above the base plate in the sub-mantle tissue, and contain mostly female reproductive tissues. **(D)** UT sections are cut close to the top of the barnacle, near the operculum, and contain lining tissue against the inside of the parietal plates, a small portion of the main body, and parts of the cirri. Scale bar = 1 mm for panels **(A–D)**. **(E–H)** Accompanying schematics depicting major anatomical features: 1. Parietal plates; 2. Opercular plates; 3. Gills; 4. Main body; 5. Digestive tract; 6. Testes; 7. Connective tissue; 8. Muscle; 9. Longitudinal canal tissue; 10. Sub-mantle tissue; 11. Adhesive layer (cuticle + proteinaceous adhesive); 12. Lateral canal tissue; 13. Baseplate; 14. Mantle cavity; 15. Epithelial cells at leading edge; 16. Ovaries; 17. Cement glands; 18. Mantle; 19. Inner shell tissue; 20. Cirri.

weights in **Supplementary Figure S1B**, particularly in the antigen blot, roughly correspond to MW increments of AaCP19-1 and suggest oligomerization. Other faint bands in the adhesive blot (lane 2, 1:100 dilution) may indicate AaCP19-1 interacting with other proteins, but we note these are absent in lane 3 (1:500 dilution). Combined, these data confirm antigen binding and positive staining in the adhesive, thus enabling a more in-depth analysis of the antigen distribution in *A. amphitrite* histological sections.

Formalin fixed paraffin embedded sections labeled with either anti-AaCP19-1 or anti-AaCP43-1 were imaged on a confocal microscope using either Cy5-conjugated primary antibodies or unlabeled primary antibodies followed by Cy5-conjugated secondary antibodies. These two methods, combined with controls of secondary antibody only, differentiated between specific and non-specific antibody labeling in the tissue sections. Imaging was performed to monitor DAPI (cell nuclei), Cy5 (AaCP19-1 and AaCP43-1), and the intrinsic autofluorescence in *A. amphitrite* previously observed using DAPI laser excitation (405 nm) in conjunction with fluorescein emission (525/50 nm) (Burden et al., 2014; Fears et al., 2018).

Based on H&E stained sections, the material at the barnacle base and closest to the substrate was consistent with a cuticle-like membrane adjacent to the cement. In transverse H&E sections near the barnacle base, this material was also consistent with the radial growth pattern observed previously (Burden et al., 2012, 2014; Golden et al., 2016; Fears et al., 2018). As AaCP19-1 and AaCP43-1 were previously identified in the *A. amphitrite* adhesive (So et al., 2016; Schultzhaus et al., 2019), antibody staining at the substrate-barnacle interface was first examined. While the characteristic strong autofluorescent signal in the fluorescein channel was seen in the basal region, no background signal was observed for the Cy5 channel (**Supplementary Figure S2**). In sagittal and transverse sections incubated with a Cy5- conjugated secondary antibody as a control, a significant amount of positive staining was observed in material at the barnacle base (**Supplementary Figure S3**). This non-specific staining precluded further examination of this basal zone with either AaCP19-1 or AaCP43-1 primary antibody.

In the sub-mantle tissue, organs defined as cement glands have traditionally been indicated as the production site for the adhesive proteins (Darwin, 1854; Lacombe and Liguori, 1969; Lacombe, 1970; Saroyan et al., 1970; Walker, 1970). These structures are dispersed within the sub-mantle tissue among the ovarioles and both features are readily identified by their distinct morphology when stained in histological sections (**Figure 2**; purple = cement glands [black arrows]; dark pink = ovaries [red arrows]; and **Supplementary Figure S3**). When stained with anti-AaCP19-1, no signal was detected within the cement glands (**Figures 3A–C**). However, positive anti-AaCP19-1 staining was

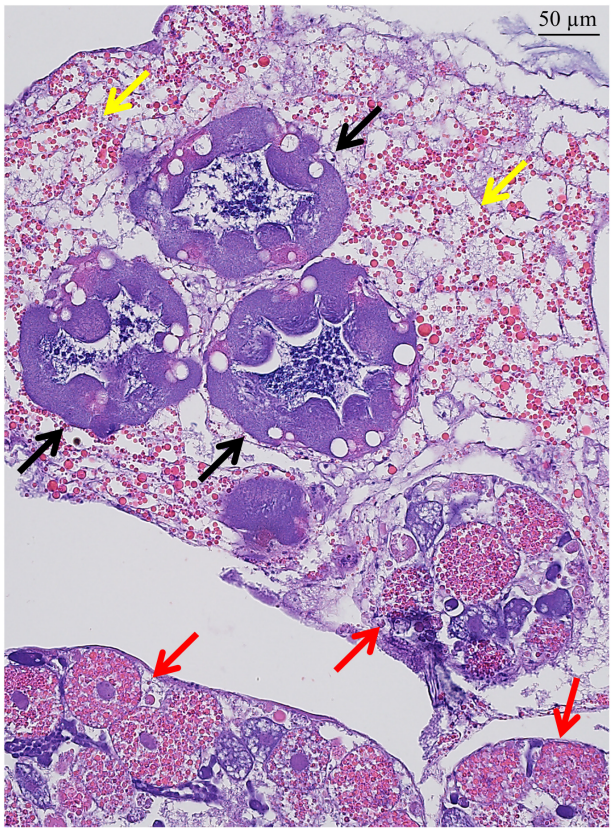

FIGURE 2 | H&E stained sub-mantle tissue features. Transverse section containing cement glands (deep purple; black arrows) and ovarioles (red arrows) with oocytes in various developmental stages surrounded by connective tissue with visible lipid granules (yellow arrows). Scale bar = 50 µm.

observed as a punctate pattern in connective tissue surrounding the cement glands and ovarioles (**Figures 3A,D**, white arrows). In addition, anti-AaCP19-1 signal was present in small cells located within, yet at the periphery of, the ovarioles (**Figures 3D–G**). These could be nursery or supporting cells that aid the developing oocytes (Fyhn and Costlow, 1975; Anderson, 1994; Wang et al., 2018). No staining within the maturing oocytes themselves was observed with anti-AaCP19-1 (**Figures 3D,E** and **Supplementary Figure S4**).

The staining pattern of α-AaCP43-1 in these same tissues was notably different. Within the cement glands, a punctate pattern of fluorescence was observed along the periphery (**Figures 3H–J**, blue arrows). In these particular sections, signal for anti-AaCP43-1 was also observed in the adjacent ovarioles (**Figures 3H,I**) with the greatest fluorescence seen in the cytoplasm of what appear to be relatively large, developing oocytes (**Figure 3H**, yellow arrows).

Outside of the sub-mantle region other distinct staining profiles were observed with both anti-AaCP19-1 and anti-AaCP43-1. For anti-AaCP19-1, relatively thin strips or linings outside of the main body and more closely associated with the tissue lining the inner side of the parietal plates (and far removed from the barnacle base) displayed strong fluorescence (**Figures 4A–G**). In most instances, the tissue lining had a distinct texture: the side of the lining not directly attached to tissue has an undulating, microvilli-like appearance though absent of nuclei (**Figures 4D,E** and **Supplementary Figures S5A,B**). These tissues were typically tens to hundreds of microns medial to the lateral edge. Another tissue lining in proximity to the longitudinal canal tissue also showed positive staining (**Figures 4F,G**), though the lining did not appear to have the undulating morphology. The main body and muscle did not show evidence of positive staining with anti-AaCP19-1. Examples for positive anti-AaCP19-1 immunostaining in other sections are included in **Supplementary Figure S5**.

Outside of the sub-mantle region containing ovarioles and cement glands, positive staining with anti-AaCP43-1 was mainly confined to a tissue lining closer to the periphery of the barnacle in both transverse and sagittal sections (**Figures 4H–O**). The stained lining was most prominent in the upper third of sagittal sections, particularly along the opercular opening. In complementary brightfield images, regions with positive staining to α-AaCP43-1 were nearly transparent, indicating little refractive index contrast either due to the thickness of those regions or the composition of tissue itself. As with α-AaCP19-1, no significant staining was observed in the main body or in muscle. Additional examples for anti-AaCP43-1 immunostaining in other sections are included in **Supplementary Figure S6**.

Proteomic Analysis of FFPE Tissue Sections

Proteomic analysis of FFPE tissue sections was conducted to complement and verify the immunohistochemical detection of AaCP19-1 and AaCP43-1, particularly in regions removed from the substrate interface. As few published studies have attempted to recover protein from FFPE tissue sections for proteomics (Longuespée et al., 2016; Alberts et al., 2018; Föll et al., 2018), we first confirmed that these methods could be adapted to barnacle tissue to identify proteins, particularly the cement proteins of interest. We chose sections where a sagittally bisected barnacle was then further sectioned to concurrently produce a series transverse and sagittal slices from either half (**Figures 1**, **4A**). We examined two adjacent pairs of sections where the sagittal section was close to the midline and contained the main body, female reproductive tissue in the sub-mantle tissue, and the interfacial material; the transverse section from the same bisected barnacle consisted mainly of interfacial material and longitudinal canal tissue (Sagittal + Basal Transverse sections [S + BT]). Note the region we identify as interfacial material in the H&E stained sections is apparent based on its location (along the barnacle-substrate interface) and eosin-rich (pink) staining.

Peptides extracted from FFPE sections were analyzed with an untargeted, shotgun acquisition method. The mass spectra produced from the S + BT sections were searched against a self-curated *A. amphitrite* protein database, as has been described previously (Fears et al., 2019). This database is composed of

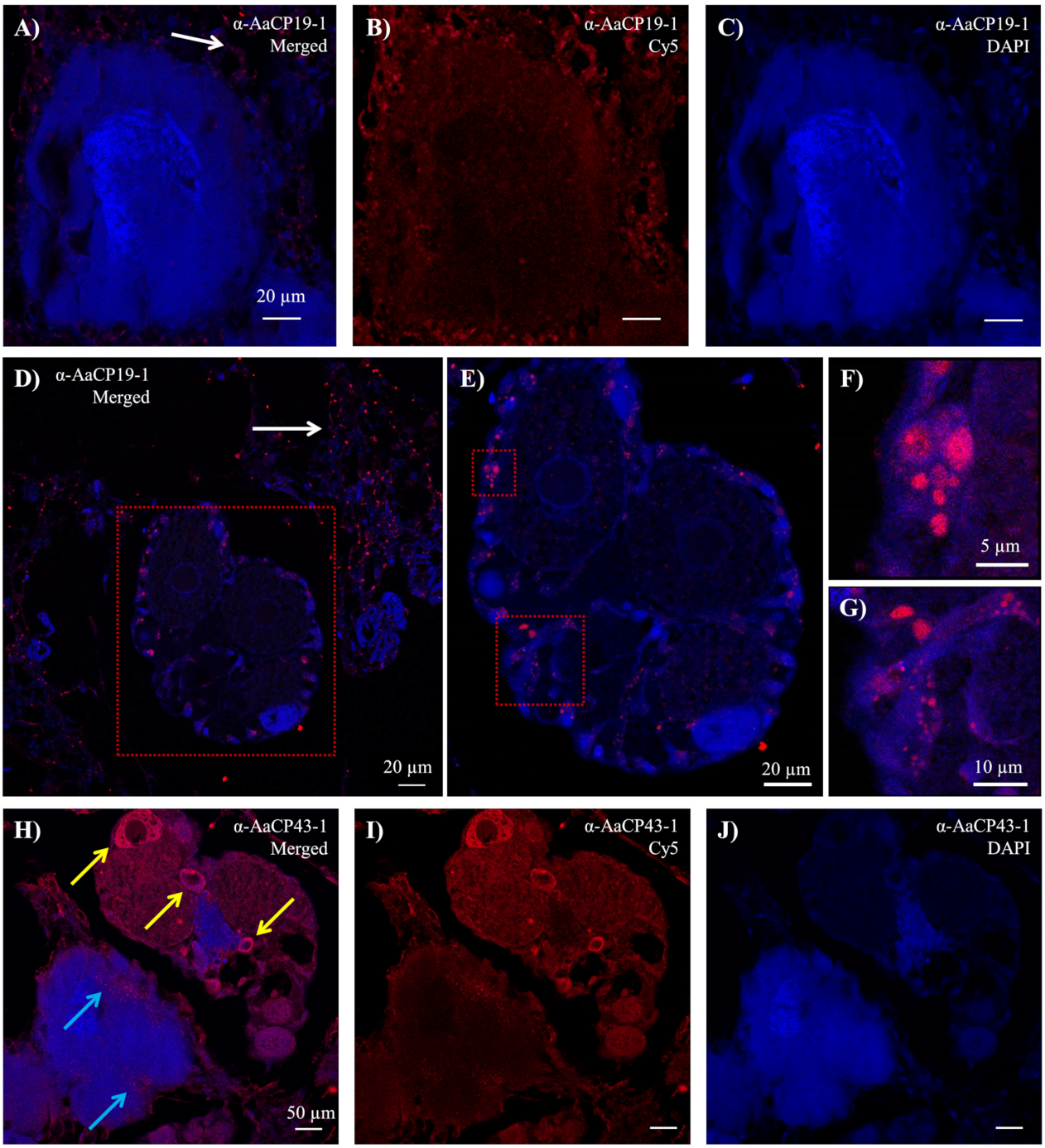

FIGURE 3 | Immunohistochemistry results from transverse sectioned sub-mantle tissue. **(A–G)** Confocal images with Cy5-labeled α-AaCP19-1. **(A)** Merged image of the **(B)** Cy5 channel showing secondary signal and the **(C)** DAPI channel of sections incubated with α-AaCP19-1. **(D–G)** Ovariole at varying magnifications showing distinct Cy5-labeled features mainly in small cells at the periphery of the ovariole. Red box in panel **(D)** is the field of view in panel **(E)**. Red boxes in panel **(E)** are the fields of view shown in panels **(F,G)**. Punctate positive staining in connective tissue is indicated in panels **(A,D)** with white arrows. **(H–J)** Confocal images with Cy5-labeled α-AaCP43-1 showing signal in both ovarioles and cement glands. **(H)** Merged image of **(I)** Cy5 channel and **(J)** DAPI channel. Punctate signal can be seen in the cement glands (blue arrows) and in the cytoplasm of large cells within ovarioles (yellow arrows).

the predicted sequences of proteins previously identified in *A. amphitrite* adhesive (Wang et al., 2015, 2018; So et al., 2016, 2017; Schultzhaus et al., 2019), two other proteins (actin and collagen) likely to be in high abundance (Schultzhaus et al., 2019), and ∼190 common contaminants. Overall, four peptides from AaCP19-1 and 18 from AaCP43-1 were identified in the S + BT

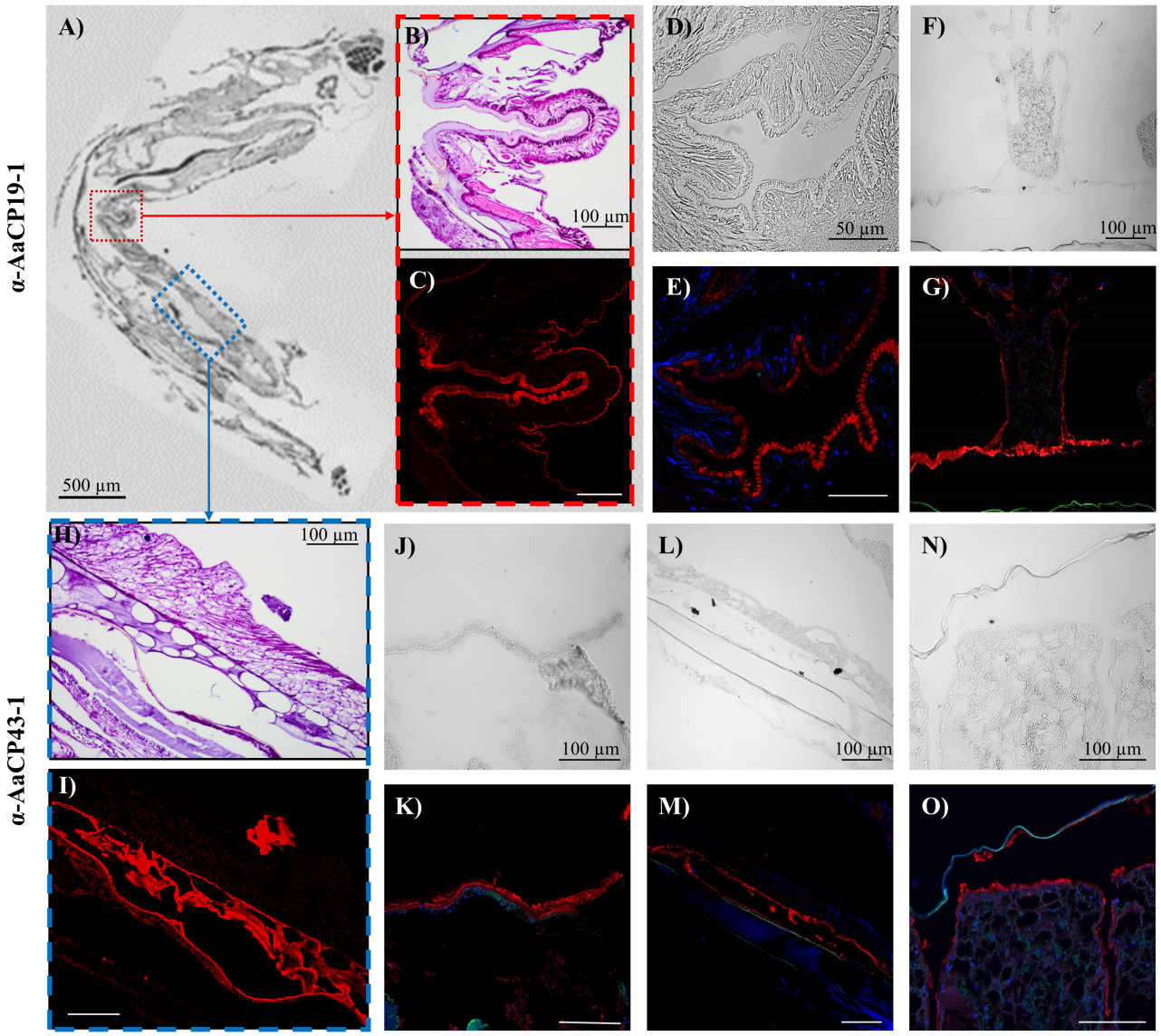

FIGURE 4 | Immunohistochemistry results for **(A–G)** α-CP19-1 and **(H–O)** α-AaCP43-1 from sections ∼130 µm from the substrate interface. **(A)** Brightfield image of transverse FFPE section containing tissue lining the inside of the shell above the sub-mantle tissue. **(B)** H&E stained and **(C)** Cy5 channel from α-AaCP19-1 stained section represented by the red box in panel **(A)**. **(D,F)** Brightfield and **(E,G)** fluorescent (DAPI and Cy5 channels) images of other transverse sections showing positive α-CP19-1 staining of the lining tissue near the operculum. **(H)** H&E stained and **(I)** Cy5 channel from α-AaCP43-1 stained section represented by the blue box in panel **(A)**. **(J,L,N)** Brightfield and **(K,M,O)** corresponding fluorescent images of α-AaCP43-1-labeled transverse sections. **(J–M)** α-AaCP43-1 stained tissue linings in proximity to the parietal shells. **(N,O)** Lining of longitudinal canal tissue staining positive for α-AaCP43-1.

sections (**Table 1**). While each of the four AaCP19-1 peptides was observed once, the AaCP43-1 peptides were identified 218 times.

With successful protein recovery and identification of AaCP19-1 and AaCP43-1 from the S + BT sections, three pooled transverse sections from three different barnacles at two locations well removed from the basis were selected for proteomics analysis (see **Figures 1A–C**, **4A**, LT and UT sections; "Materials and Methods"). The UT samples were taken near the opercular opening and contain cirri, the top of the prosoma, muscle, and tissue that lines the shell. The LT sections were taken near, though above, the basis and contain ovaries, muscle, longitudinal canal tissue, the bottom of the prosoma, and some cuticular and/or cement material.

AaCP43-1 was identified in both LT and UT sections while AaCP19-1 was not identified in the UT sections (**Table 1**). More spectra were assigned to AaCP43-1 in all cases, especially in the S + BT sample where the base material was abundant. We then developed a targeted fragmentation method to specifically enhance the chances for identifying AaCP19-1 and AaCP43-1 peptides. The targeted fragmentation method resulted in similar patterns of identification for both proteins, confirming the untargeted results (**Supplementary File S2**).

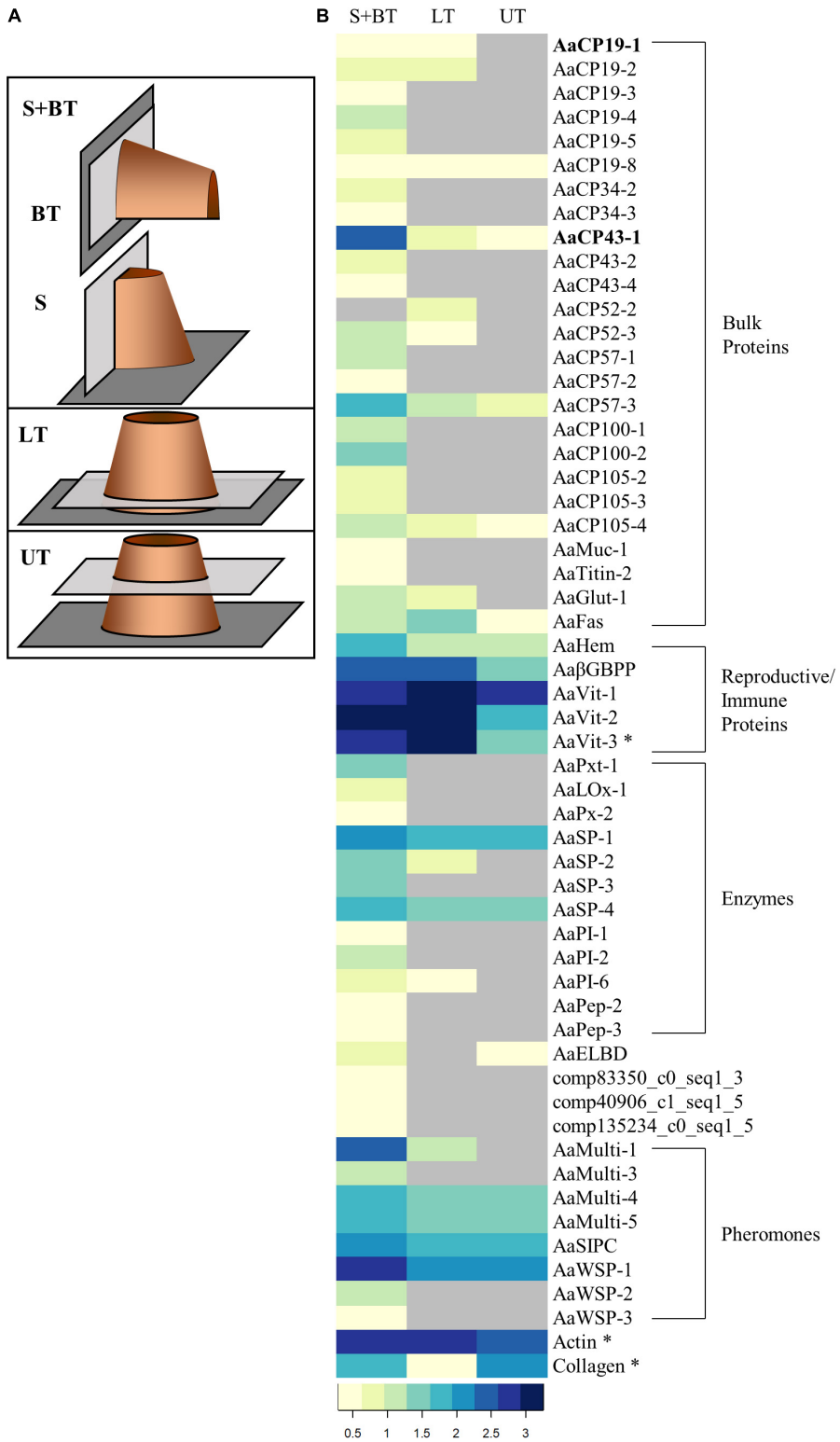

FIGURE 5 | Proteomic analysis of FFPE sections. **(A)** Schematic representations indicating the location (light gray rectangles) of the sections along a barnacle (orange cylinder) settled on a substrate (dark gray rectangle) analyzed for proteomics. Sagittal = S; BT = Basal Transverse; LT = Lower Transverse; UT = Upper Transverse. S and BT sections were combined (S + BT). The locations indicated here match exactly with the sections in **Figure 1**. **(B)** Heatmap illustrating total spectrum counts (log10 transformed) for S + BT, LT, and UT FFPE sections. The proteins are grouped by predictive function: bulk proteins that compose adhesive at the interface; proteins that play a role in reproduction and/or immunity; and pheromones. Gray cells indicate no identification. Asterisks indicate proteins that have not been identified in the adhesive previously. AaCP19-1 and AaCP43-1 identifiers are in bold.

TABLE 1 | Results of proteomic analysis of FFPE sections.

	AaCP19-1		AaCP43-1	
Sample	**PSM[A]**	**Peptides[B]**	**PSM[A]**	**Peptides[B]**
Sagittal + Basal Transverse (S + BT)	4	4	218	18
Lower Transverse (LT)	3	3	5	2
Upper Transverse (UT)	0	0	4	3

[A]PSM = peptide spectrum match. [B]Peptides = unique peptides.

As a complementary method to immunohistochemistry, our proteomics approach allows for the recovery and identification of many proteins without the need for antibodies. Therefore, we assessed the FFPE sections for the presence of all other proteins previously identified in the adhesive (So et al., 2016; Schultzhaus et al., 2019). The results are shown in **Figure 5** as a heat map of the log10 transformed total spectrum counts per protein. Proteins are grouped by predicted function: *bulk proteins* that make up the adhesive; proteins that play a role in both *immunity and reproduction* and are likely circulated via the hemolymph; *enzymes* involved in a range of processes that likely contribute to molting; and *pheromones*. Of the 56 proteins identified, 29 were only observed in the S + BT sections that included material at the interface between the organism's basis and the underlying substrate. The lack of identification in sections with no interfacial material indicates that these proteins may be restricted to the basis. The remaining proteins can be identified in tissues throughout the barnacle and are therefore not unique to the base, where cementing occurs.

For the 26 identified bulk proteins, all but one were identified in the S + BT sections. The majority of the bulk proteins (15) were only identified in the S + BT sections, five were also observed in the LT sections, and six were identified in all sections. The reproductive/immune related proteins were identified throughout in all sections, with the vitellogenin proteins, AaVit, showing an elevated identification in tissues where the ovaries are located, i.e., the S + BT and LT sections. Eight of the twelve enzymes were also restricted to the S + BT samples, while two of the serine proteases (AaSP-1 and -4) had a broader distribution in all sections. Several of the pheromones (AaMulti-4 and -5, AaSIPC, and AaWSP-1) were identified in all sections, while the other pheromones were restricted to the S + BT samples. Actin and collagen were identified in all sections.

DISCUSSION

Since the initial isolation and identification of proteins from acorn barnacle plaques (Kamino et al., 1996), there has been much speculation as to the mechanism of cement formation and the origins of the proteins responsible for the robust adhesive properties at the acorn barnacle-substrate interface. Further, the nomenclature developed for proteins first identified in the barnacle adhesive layer as "cement proteins" has, at times, come to imply that any materials identified at the interface could be key components of the adhesion mechanism despite the lack of functional assays to provide supporting evidence. This terminology also implies that the proteins found at the interface and in the adhesive are restricted to this location.

The advancement of observation techniques and analytical tools applied to understanding the acorn barnacle interface and cement has led to a marked increase in the number of components identified at this layer (Wang et al., 2015; So et al., 2016, 2017; Schultzhaus et al., 2019) and their associated activities (Golden et al., 2016; So et al., 2017). In some cases, the proteins identified at the interface are unique to barnacles, though others (e.g., enzymes) are known with established roles in functions such as signaling cascades for immunity and cuticle sclerotization. A plethora of hypotheses as to the mechanisms underlying adhesion in acorn barnacles has been proposed, including hydrophobic hydrogen bond interactions (Kamino et al., 2012), amyloid-like nanostructures (Kamino et al., 1996; Sullan et al., 2009; Barlow et al., 2010), wound healing involving serine proteases (Dickinson et al., 2009; Essock-Burns et al., 2019), and spider silk homology (So et al., 2016). Under this backdrop, we sought to add another piece to the puzzle of understanding acorn barnacle cement by analyzing whether "cement proteins" identified in the adhesive interface in *A. amphitrite* are unique to this basal region or found in other locations of the acorn barnacle.

Here, we use antibodies developed against AaCP19-1 and AaCP43-1 to examine FFPE sections. These antibodies show specific binding in western blots of solubilized cement and purified proteins [see **Supplementary Figure S1** and refs (So et al., 2017, 2019)]. Our immunohistochemistry results and protein analysis of FFPE sections provide two independent techniques to demonstrate that these cement proteins are not exclusive to the adhesive interface, but rather are found in select tissues well removed from the basal region of *A. amphitrite*. Both appear to localize to at least the multi-layered connective material roughly located along the interior linings of the shell plates.

In addition to material lining the shell plates, immunostaining for AaCP19-1 indicates its presence along the lining of the longitudinal canal tissue and in discrete spots around the periphery of ovarioles and the surrounding tissue (**Figure 4**). Immunostaining of AaCP43-1 was mainly observed as a separate set of tissue and linings, the latter appearing as a layer close to the interior boundary of parietal plates in transverse sections of *A. amphitrite* (**Figures 4H–O**). The material was nearly transparent in brightfield images, thus showing a distinction from the linings with positive α-AaCP19-1 staining.

As noted, non-specific binding of secondary antibodies was observed in the base region of the barnacle (**Supplementary Figure S2**), particularly the relatively thick, eosinophilic-rich region in the H&E stained slides (**Figure 1A**). Examination of transverse and sagittal sections, combined with our previous observations of the base region (Burden et al., 2014; Fears et al., 2018; Wang et al., 2018) reveals this material to be chitinous and growing in a radial, ringed pattern as the barnacle extends its interfacial surface area in a manner synchronized with its molt cycle.

Recovery and identification of peptides and proteins from FFPE sections using mass spectrometry provided an independent method to verify the presence of specific proteins in non-cementing regions of *A. amphitrite*. While recovery of protein

from the sections was an accomplishment in itself, the identification of cement proteins from transverse sections tens to hundreds of microns from the barnacle base provide support to our findings that many proteins first identified in the cementing region of *A. amphitrite* are not exclusive to the adhesive interface.

In identifying the proteins in non-cementing regions of the barnacle, a small, targeted database was used for spectra assignment. While this restricted database limits the survey of all proteins that may be identified from material recovered from the FFPE sections, it enabled targeted PSM assignments to proteins of interest, which were previously identified by our group from larger-scale "shotgun" studies (Wang et al., 2015; So et al., 2016; Schultzhaus et al., 2019). As PSM assignments met or exceeded experimental criteria used in previous studies, this analysis increases the confidence of correct peptide-spectrum assignment in our workflow.

When considering the distribution of all the proteins examined from the smaller database, it becomes apparent that most of the proteins are identified in the S + BT sections where the adhesive layer was prominent. Certain cement proteins (AaCP19-8, AaCP43-1, AaCP57-3, and AaCP105-4), the vitellogenins and immune related proteins, enzymes (AaSP-1 and -4), and many of the pheromones were identified in all three tissue sections examined. As expected, all but one of the identified proteins from the adhesive-specific database were found in the S&T section. However, about half of the proteins in **Figure 5** were also found elsewhere, including several that were previously implicated in cementing/adhesion (So et al., 2016). The database used for protein assignment was composed almost completely of proteins identified in the adhesive, and their biased identification in samples containing the interface region suggests either enrichment or restriction of these proteins at the interface.

These data and analyses provide new ground truth observations that contradict long-held claims about the nature and uniqueness of the major components of the cement layer in acorn barnacles. For the most part, the origin, modification, transport, and even the physiological roles of cement proteins in acorn barnacles have not been systematically investigated. The current study provides a launching point from which to begin to address some of these knowledge gaps. Our analysis shows, for the first time, that certain proteins initially identified in the cement layer of *A. amphitrite* are likely *enriched* in this region, but are not *unique* to this location. The results for AaCP43-1 indicate this protein may indeed be critical for adhesion, though its presence elsewhere implies a function beyond the interface. Immunostaining of AaCP19-1 also implies broader distribution, although the lack of identified AaCP19-1 peptides in the proteomic analysis fails to confirm the staining patterns. To the latter point, these results highlight the challenges associated with several aspects of the proteomic analysis from FFPE sections. For example, established methods for protein recovery from FFPE sections are not well established. There are also limitations in the amount of material in the sections themselves, particularly if the proteins originate from thin tissues within the sections, and the amount and type of proteins recovered (even with pooled samples). This last point may apply more severely to low molecular weight proteins, i.e., the AaCP19-like proteins. Combined, these factors complicate the interpretation of negative results from the proteomic analysis.

The expansion of the number of proteins identified at the adhesive interface (Wang et al., 2015; So et al., 2016; Schultzhaus et al., 2019) combined with a more comprehensive understanding of the process of growth at the leading edge of the acorn barnacle basis (Burden et al., 2012, 2014; Golden et al., 2016; Fears et al., 2018) deepens the knowledge of how the robust interface is formed. Despite this progress, a large number of proteins in acorn barnacles do not share significant homology with any known proteins and, therefore, remain uncharacterized. The scope of this issue has been partly reduced with the publication of the genomes of a limited number of marine arthropods (Colbourne et al., 2011; Kao et al., 2016; Zhang et al., 2019) and, more recently, a draft genome of *A. amphitrite* itself (Kim et al., 2019). We note the other species are still relatively distant relatives and highlight the need for high-quality genomic sequencing in *A. amphitrite*. Such an effort will be a next major step toward advancing to the goal of a complete understanding of the protein components of cement and the factors that contribute to adhesion.

The results outlined here provide the first concrete observations that not all barnacle cement proteins are necessarily unique to the substrate interface, but rather can be found in tissue and tissue linings throughout the barnacle. These findings support the recent work of Essock-Burns et al. that showed evidence of oxidative activity in the cuticle of *A. amphitrite*, indicating enzyme enrichment in tissues other than just the adhesive interface (Essock-Burns et al., 2019). It is possible that certain proteins found in the cement are adapted or modified to facilitate adhesive properties at the substrate interface. Given the cuticle-like material at the interface, proteinaceous barnacle cement could be viewed as a modified boundary to the cuticle of arthropods, which is typically composed of multiple layers including an epidermis, endocuticle, exocuticle, and epicuticle. Comparisons of the cuticle associated with the upper part of the animal (with an obvious exuvium synchronized with the molt cycle) with acorn barnacle plaques are a current area of investigation in our research group and may shed further light on understanding the robust properties of the obscured cement of acorn barnacles.

For some time, it was assumed that cement proteins in acorn barnacles were unique to the interfacial cement. While these proteins were first identified and isolated from the barnacle cement, their functional role is uncharacterized. We have shown via immunohistochemistry and proteomic analysis of FFPE tissue sections that barnacle "cement proteins" and other related proteins are in fact distributed throughout the animal in what appear to be relatively specific tissues in diverse locations. While certain proteins are more likely to be present in the barnacle basis, other presumptive "cement" proteins appear to be present in tissues from sections well removed from the substrate interface. Combined, these results help refine the potential key players at the adhesive interface and which materials may fulfill a more general supporting role in the various tissues and tissue linings in the barnacle.

DATA AVAILABILITY STATEMENT

The datasets presented in this study can be found in online repositories. The names of the repository/repositories and accession number(s) can be found below: https://chorusproject.org/, Project#3538.

ETHICS STATEMENT

Ethical review and approval was not required for this study at the U.S. Naval Research Laboratory since the acorn barnacle *A. amphitrite* is classified as a fouling organism and nuisance marine invertebrate.

AUTHOR CONTRIBUTIONS

CW conceived and planned the histology and immunofluorescence confocal microscopy experiments. CW, SP, and MS prepared immunostained tissue sections. JNS, CW, DP, CMS, SP, and MS contributed to confocal imaging and analysis. CRS and JMS prepared and analyzed the immunoblots. JNS developed and implemented the histological protein recovery for identification and analysis. JNS, DL, and JH provided proteomic analysis. JNS and CMS wrote the manuscript with input from all authors. CRS, CT, GD, and KW provided critical editing of the manuscript. KW and CMS supervised the effort. All authors contributed to the article and approved the submitted version.

FUNDING

Funding for this work was provided by internal Basic Research programs (Work Units 1G21 and 1L73) at the U.S. Naval Research Laboratory.

ACKNOWLEDGMENTS

JNS acknowledges the National Research Council for Post-Doctoral Associateship. DP acknowledges the American Society for Engineering Education for a Post-Doctoral Fellowship. SP and MS acknowledge the Naval Research Enterprise Internship Program for their summer internships. Barnacles were kindly provided by Dr. Daniel Rittschof, the Norman L. Christensen Distinguished Professor of Environmental Sciences at Duke University's Nicholas School of the Environment, with support from the Office of Naval Research. We also acknowledge the histological services provided by Dr. Deborah Barry at the Histopathology and Tissue Shared Resource at the Georgetown University Lombardi Comprehensive Cancer Center.

SUPPLEMENTARY MATERIAL

The Supplementary Material for this article can be found online at: https://www.frontiersin.org/articles/10.3389/fmars.2020.586281/full#supplementary-material

Supplementary Figure 1 | Immunoblot analysis of *A. amphitrite* adhesive with the polyclonal antibody α-AaCP19-1.

Supplementary Figure 2 | Fluorescence confocal images of bisected *A. amphitrite* demonstrating no fluorescent bleed-through in the CY5 (red) channel.

Supplementary Figure 3 | Cy5-labeled secondary antibody controls on *A. amphitrite* sections.

Supplementary Figure 4 | Transverse *A. amphitrite* sections of sub-mantle and longitudinal canal tissue stained with either Cy5-conjugated α-AaCP19-1 or α-AaCP43-1.

Supplementary Figure 5 | Transverse *A. amphitrite* sections stained with Cy5-conjugated α-AaCP19-1 highlighting different tissues with positive signal.

Supplementary Figure 6 | Transverse *A. amphitrite* sections stained with Cy5-conjugated α-AaCP43-1 highlighting various tissue linings with positive signal.

Supplementary Table 1 | List of AaCP19-1 and AaCP43-1 peptide sequences submitted for targeted fragmentation.

Supplementary File 1 | Word document with a detailed description of the Mass Spectrometry methods.

Supplementary File 2 | Excel spreadsheet of MS analysis comparing the protein identification of the targeted and untargeted methods.

REFERENCES

Alberts, D., Pottier, C., Smargiasso, N., Baiwir, D., Mazzucchelli, G., Delvenne, P., et al. (2018). MALDI Imaging−guided microproteomic analyses of heterogeneous breast tumors—a pilot study. *Proteomics Clin. Appl.* 12:1700062. doi: 10.1002/prca.201700062

Anderson, D. T. (1994). *Barnacles: Structure, Function, Development and Evolution*. London: Chapman & Hall.

Barlow, D. E., Dickinson, G. H., Orihuela, B., Kulp, J. L. III, Rittschof, D., and Wahl, K. J. (2010). Characterization of the adhesive plaque of the barnacle *Balanus amphitrite*: amyloid-like nanofibrils are a major component. *Langmuir* 26, 6549–6556. doi: 10.1021/la9041309

Burden, D. K., Barlow, D. E., Spillmann, C. M., Orihuela, B., Rittschof, D., Everett, R., et al. (2012). Barnacle *Balanus amphitrite* adheres by a stepwise cementing process. *Langmuir* 28, 13364–13372. doi: 10.1021/la301695m

Burden, D. K., Spillmann, C. M., Everett, R. K., Barlow, D. E., Orihuela, B., Deschamps, J. R., et al. (2014). Growth and development of the barnacle *Amphibalanus amphitrite*: time and spatially resolved structure and chemistry of the base plate. *Biofouling* 30, 799–812. doi: 10.1080/08927014.2014.930736

Clare, A. S., and Høeg, J. T. (2008). *Balanus amphitrite* or *Amphibalanus amphitrite?* A note on barnacle nomenclature. *Biofouling* 24, 55–57. doi: 10.1080/08927010701830194

Clare, A. S., and Rittschof, D. (1989). What's in a name? *Nature* 338:627.

Colbourne, J. K., Pfrender, M. E., Gilbert, D., Thomas, W. K., Tucker, A., Oakley, T. H., et al. (2011). The ecoresponsive genome of *Daphnia pulex*. *Science* 331, 555–561.

Darwin, C. (1854). *A Monograph on The Sub-Class Cirripedia, With Figures of All The Species. Living Cirripedia, The Balanidae, (or Sessile Cirripedes); The Verrucidae*, Vol. 2. London: The Ray Society.

Dean, S. N., Rimmer, M. A., Turner, K. B., Phillips, D. A., Caruana, J. C., Hervey, W. J., et al. (2020). *Lactobacillus acidophilus* membrane vesicles as a vehicle of bacteriocin delivery. *Front. Microbiol.* 11:710. doi: 10.3389/fmicb.2020.00710

Dickinson, G. H., Vega, I. E., Wahl, K. J., Orihuela, B., Beyley, V., Rodriguez, E. N., et al. (2009). Barnacle cement: a polymerization model based on evolutionary concepts. *J. Exp. Biol.* 212, 3499–3510. doi: 10.1242/jeb.029884

Essock-Burns, T., Soderblom, E. J., Orihuela, B., Moseley, M. A., and Rittschof, D. (2019). Hypothesis testing with proteomics: a case study using wound healing

mechanisms in fluids associated with barnacle glue. *Front. Mar. Sci.* 6:343. doi: 10.3389/fmars.2019.00343

Fears, K. P., Barnikel, A., Wassick, A., Ryou, H., Schultzhaus, J. N., Orihuela, B., et al. (2019). Adhesion of acorn barnacles on surface-active borate glasses. *Phil. Trans. R. Soc. B* 374, 20190203. doi: 10.1098/rstb.2019.0203

Fears, K. P., Orihuela, B., Rittschof, D., and Wahl, K. J. (2018). Acorn barnacles secrete phase−separating fluid to clear surfaces ahead of cement deposition. *Adv. Sci.* 5:1700762. doi: 10.1002/advs.201700762

Föll, M. C., Fahrner, M., Oria, V. O., Kühs, M., Biniossek, M. L., Werner, M., et al. (2018). Reproducible proteomics sample preparation for single FFPE tissue slices using acid-labile surfactant and direct trypsinization. *Clin. Proteom.* 15:11.

Fyhn, U. E., and Costlow, J. D. (1975). Tissue cultures of cirripeds. *Biol. Bull.* 149, 316–330. doi: 10.2307/1540529

Fyhn, U. E., and Costlow, J. D. (1976). A histochemical study of cement secretion during the intermolt cycle in barnacles. *Biol. Bull.* 150, 47–56. doi: 10.2307/1540588

Golden, J. P., Burden, D. K., Fears, K. P., Barlow, D. E., So, C. R., Burns, J., et al. (2016). Imaging active surface processes in barnacle adhesive interfaces. *Langmuir* 32, 541–550. doi: 10.1021/acs.langmuir.5b03286

He, L.-S., Zhang, G., Wang, Y., Yan, G.-Y., and Qian, P.-Y. (2018). Toward understanding barnacle cementing by characterization of one cement protein-100kDa in *Amphibalanus amphitrite*. *Biochem. Biophys. Res. Commun.* 495, 969–975. doi: 10.1016/j.bbrc.2017.11.101

Hervey, W. J., Khalsa-Moyers, G., Lankford, P. K., Owens, E. T., McKeown, C. K., Lu, T. Y., et al. (2009). Evaluation of affinity-tagged protein expression strategies using local and global isotope ratio measurements. *J. Prot. Res.* 8, 3675–3688. doi: 10.1021/pr801088f

Jonker, J.-L., Abram, F., Pires, E., Coelho, A. V., Grunwald, I., and Power, A. M. (2014). Adhesive proteins of stalked and acorn barnacles display homology with low sequence similarities. *PLoS One* 9:e108902. doi: 10.1371/journal.pone.0108902

Kamino, K. (2013). Mini-review: barnacle adhesives and adhesion. *Biofouling* 29, 735–749. doi: 10.1080/08927014.2013.800863

Kamino, K., Inoue, K., Maruyama, T., Takamatsu, N., Harayama, S., and Shizuri, Y. (2000). Barnacle cement proteins: importance of disulfide bonds in their insolubility. *J. Biol. Chem.* 275, 27360–27365.

Kamino, K., Nakano, M., and Kanai, S. (2012). Significance of the conformation of building blocks in curing of barnacle underwater adhesive. *FEBS. J.* 279, 1750–1760. doi: 10.1111/j.1742-4658.2012.08552.x

Kamino, K., Odo, S., and Maruyama, T. (1996). Cement proteins of the acorn-barnacle, *Megabalanus rosa*. *Biol. Bull.* 190, 403–409. doi: 10.2307/1543033

Kao, D., Lai, A. G., Stamataki, E., Rosic, S., Konstantinides, N., Jarvis, E., et al. (2016). The genome of the crustacean *Parhyale hawaiensis*, a model for animal development, regeneration, immunity and lignocellulose digestion. *Elife* 5:e20062.

Kim, J.-H., Kim, H., Kim, H., Chan, B. K., Kang, S., and Kim, W. (2019). Draft genome assembly of a fouling barnacle, *Amphibalanus amphitrite* (Darwin, 1854): the first reference genome for Thecostraca. *Front. Ecol. Evol.* 7:465.

Lacombe, D. (1970). A comparative study of the cement glands in some balanid barnacles (Cirripedia, Balanidae). *Biol. Bull.* 139, 164–179. doi: 10.2307/1540134

Lacombe, D., and Liguori, V. R. (1969). Comparative histological studies of the cement apparatus of *Lepas anatifera* and *Balanus tintinnabulum*. *Biol. Bull.* 137, 170–180. doi: 10.2307/1539940

Lin, H.-C., Wong, Y. H., Tsang, L. M., Chu, K. H., Qian, P.-Y., and Chan, B. K. (2014). First study on gene expression of cement proteins and potential adhesion-related genes of a membranous-based barnacle as revealed from Next-Generation Sequencing technology. *Biofouling* 30, 169–181. doi: 10.1080/08927014.2013.853051

Longuespée, R., Alberts, D., Pottier, C., Smargiasso, N., Mazzucchelli, G., Baiwir, D., et al. (2016). A laser microdissection-based workflow for FFPE tissue microproteomics: important considerations for small sample processing. *Methods* 104, 154–162. doi: 10.1016/j.ymeth.2015.12.008

López-Ferrer, D., Petritis, K., Hixson, K. K., Heibeck, T. H., Moore, R. J., Belov, M. E., et al. (2008). Application of pressurized solvents for ultrafast trypsin hydrolysis in proteomics: proteomics on the fly. *J. Prot. Res.* 7, 3276–3281. doi: 10.1021/pr7008077

Nakano, M., and Kamino, K. (2015). Amyloid-like conformation and interaction for the self-assembly in barnacle underwater cement. *Biochemistry* 54, 826–835. doi: 10.1021/bi500965f

Naldrett, M., and Kaplan, D. (1997). Characterization of barnacle (*Balanus eburneus* and *B. cenatus*) adhesive proteins. *Mar. Biol.* 127, 629–635. doi: 10.1007/s002270050053

Naldrett, M. J. (1993). The importance of sulphur cross-links and hydrophobic interactions in the polymerization of barnacle cement. *J. Mar. Biol. Associat. U. K.* 73, 689–702. doi: 10.1017/s0025315400033221

Pitombo, F. B. (2004). Phylogenetic analysis of the Balanidae (Cirripedia. Balanomorpha). *Zool. Scrip.* 33, 261–276. doi: 10.1111/j.0300-3256.2004.00145.x

Power, A. M. (2010). *Mechanisms of Adhesion in Adult Barnacles. Biological Adhesive Systems: From Nature to Technical and Medical Application*. Wien: Springer-Verlag, 153–168.

Ramsay, D. B., Dickinson, G. H., Orihuela, B., Rittschof, D., and Wahl, K. J. (2008). Base plate mechanics of the barnacle *Balanus amphitrite* (= *Amphibalanus amphitrite*). *Biofouling* 24, 109–118. doi: 10.1080/08927010701882112

Rittschof, D., Orihuela, B., Stafslein, S., Daniels, J., Christianson, D., Chisholm, B., et al. (2008). Barnacle reattachment: a tool for studying barnacle adhesion. *Biofouling* 24, 1–9. doi: 10.1080/08927010701784920

Rocha, M., Antas, P., Castro, L. F. C., Campos, A., Vasconcelos, V., Pereira, F., et al. (2018). Comparative analysis of the adhesive proteins of the adult stalked goose barnacle *Pollicipes pollicipes* (Cirripedia: Pedunculata). *Mar. Biotechnol.* 18, 1–14.

Saroyan, J., Lindner, E., and Dooley, C. (1970). Repair and reattachment in the balanidae as related to their cementing mechanism. *Biol. Bull.* 139, 333–350. doi: 10.2307/1540088

Schultzhaus, J. N., Dean, S. N., Leary, D. H., Hervey, W. J., Fears, K. P., Wahl, K. J., et al. (2019). Pressure cycling technology for challenging proteomic sample processing: application to barnacle adhesive. *Integrat. Biol.* 11, 235–247. doi: 10.1093/intbio/zyz020

So, C. R., Fears, K. P., Leary, D. H., Scancella, J. M., Wang, Z., Liu, J. L., et al. (2016). Sequence basis of barnacle cement nanostructure is defined by proteins with silk homology. *Sci. Rep.* 6:36219.

So, C. R., Scancella, J. M., Fears, K. P., Essock-Burns, T., Haynes, S. E., Leary, D. H., et al. (2017). Oxidase activity of the barnacle adhesive interface involves peroxide-dependent catechol oxidase and lysyl oxidase enzymes. *ACS Appl. Mater. Interfaces* 9, 11493–11505. doi: 10.1021/acsami.7b01185

So, C. R., Yates, E. A., Estrella, L. A., Fears, K. P., Schenck, A. M., Yip, C. M., et al. (2019). Molecular recognition of structures is key in the polymerization of patterned barnacle adhesive sequences. *ACS Nano* 13, 5172–5183. doi: 10.1021/acsnano.8b09194

Sullan, R. M. A., Gunari, N., Tanur, A. E., Yuri, C., Dickinson, G. H., Orihuela, B., et al. (2009). Nanoscale structures and mechanics of barnacle cement. *Biofouling* 25, 263–275. doi: 10.1080/08927010802688095

Taitt, C. R., North, S. H., and Kulagina, N. V. (2009). Antimicrobial peptide arrays for detection of inactivated biothreat agents. *Methods Molec. Biol.* 570, 233–255. doi: 10.1007/978-1-60327-394-7_11

Tao, F., Li, C., Smejkal, G., Lazarev, A., Lawrence, N., and Schumacher, R. T. (2007). Pressure cycling technology (PCT) applications in extraction of biomolecules from challenging biological samples. *High Press. Biosci. Biotechnol.* 1, 166–173.

Urushida, Y., Nakano, M., Matsuda, S., Inoue, N., Kanai, S., Kitamura, N., et al. (2007). Identification and functional characterization of a novel barnacle cement protein. *FEBS J.* 274, 4336–4346. doi: 10.1111/j.1742-4658.2007.05965.x

Walker, G. (1970). The histology, histochemistry and ultrastructure of the cement apparatus of three adult sessile barnacles. *Elminius modestus*, *Balanus balanoides* and *Balanus hameri*. *Mar. Biol.* 7, 239–248. doi: 10.1007/bf00367494

Wang, C., Schultzhaus, J. N., Taitt, C. R., Leary, D. H., Shriver-Lake, L. C., Snellings, D., et al. (2018). Characterization of longitudinal canal tissue in the

acorn barnacle *Amphibalanus amphitrite*. *PLoS One* 13:e0208352. doi: 10.1371/journal.pone.0208352

Wang, Z., Leary, D. H., Liu, J., Settlage, R. E., Fears, K. P., North, S. H., et al. (2015). Molt-dependent transcriptomic analysis of cement proteins in the barnacle *Amphibalanus amphitrite*. *BMC Genom.* 16:859.

Warnes, G. R., Bolker, B., Bonebakker, L., Gentleman, R., Liaw, W. H. A., Lumley, T., et al. (2015). *gplots: Various R Programming Tools for Plotting Data*. Available online at: https://github.com/talgalili/gplots (accessed January 15, 2020).

Wendt, D. E., Kowalke, G. L., Kim, J., and Singer, I. L. (2006). Factors that influence elastomeric coating performance: the effect of coating thickness on basal plate morphology, growth and critical removal stress of the barnacle *Balanus amphitrite*. *Biofouling* 22, 1–9. doi: 10.1080/08927010500499563

Zhang, X., Yuan, J., Sun, Y., Li, S., Gao, Y., Yu, Y., et al. (2019). Penaeid shrimp genome provides insights into benthic adaptation and frequent molting. *Nat. Commun.* 10:356.

Conflict of Interest: The authors declare that the research was conducted in the absence of any commercial or financial relationships that could be construed as a potential conflict of interest.

Citation: Schultzhaus JN, Wang C, Patel S, Smerchansky M, Phillips D, Taitt CR, Leary DH, Hervey J, Dickinson GH, So CR, Scancella JM, Wahl KJ and Spillmann CM (2020) Distribution of Select Cement Proteins in the Acorn Barnacle Amphibalanus amphitrite. Front. Mar. Sci. 7:586281. doi: 10.3389/fmars.2020.586281